



# CHORUS

This is the accepted manuscript made available via CHORUS. The article has been published as:

## Spin-Torque Ferromagnetic Resonance in W/Co-Fe-B/W/Co-Fe-B/MgO Stacks

Congli He, Guoqiang Yu, Cecile Grezes, Jiafeng Feng, Zhen Zhao, Seyed Armin Razavi, Qiming Shao, Aryan Navabi, Xiang Li, Qing Lin He, Mengyin Li, Jia Zhang, Kin L. Wong, Dan Wei, Guangyu Zhang, Xiufeng Han, Pedram Khalili Amiri, and Kang L. Wang

Phys. Rev. Applied **10**, 034067 — Published 28 September 2018

DOI: [10.1103/PhysRevApplied.10.034067](https://doi.org/10.1103/PhysRevApplied.10.034067)

## **Spin-torque ferromagnetic resonance in W/CoFeB/W/CoFeB/MgO stacks**

Congli He<sup>1,2,3</sup>, Guoqiang Yu<sup>2\*</sup>, Cecile Grezes<sup>3</sup>, Jiafeng Feng<sup>2</sup>, Zhen Zhao<sup>3,4</sup>, Seyed Armin Razavi<sup>3</sup>, Qiming Shao<sup>3</sup>, Aryan Navabi<sup>3</sup>, Xiang Li<sup>3</sup>, Qing Lin He<sup>3</sup>, Mengyin Li<sup>5</sup>, Jia Zhang<sup>5</sup>, Kin L. Wong<sup>3</sup>, Dan Wei<sup>4</sup>, Guangyu Zhang<sup>2</sup>, Xiufeng Han<sup>2\*</sup>, Pedram Khalili Amiri<sup>3</sup> and Kang L. Wang<sup>3,6,7\*</sup>

<sup>1</sup>Institute of Advanced Materials, Beijing Normal University, Beijing 100875, China

<sup>2</sup>Beijing National Laboratory for Condensed Matter Physics, Institute of Physics,  
Chinese Academy of Sciences, Beijing 100190, China

<sup>3</sup>Department of Electrical and Computer Engineering, University of California, Los  
Angeles, California 90095, United States

<sup>4</sup>Key Laboratory of Advanced Materials (MOE), School of Materials Science and  
Engineering, Tsinghua University, Beijing 100084, China

<sup>5</sup>School of Physics and Wuhan National High Magnetic Field Center, Huazhong  
University of Science and Technology, 430074 Wuhan, China

<sup>6</sup>Department of Physics & Astronomy, University of California, Los Angeles,  
California 90095, United States

<sup>7</sup>Department of Materials Science Engineering, University of California, Los Angeles,  
California 90095, United States

Email address: [guoqiangyu@iphy.ac.cn](mailto:guoqiangyu@iphy.ac.cn), [xfhan@iphy.ac.cn](mailto:xfhan@iphy.ac.cn), [wang@ee.ucla.edu](mailto:wang@ee.ucla.edu)

We investigate the magnetic properties of as-grown and annealed W/CoFeB/W(insertion)/CoFeB/MgO stacks with different thicknesses of CoFeB layers and W insertion layers using spin-torque ferromagnetic resonance (ST-FMR) technique. The dependences of perpendicular magnetic anisotropy (PMA), damping constant, and interlayer exchange coupling on the annealing, CoFeB layer thicknesses, and W insertion layer thicknesses are systematically studied. The PMA is strongly enhanced after annealing at 400 °C. Nevertheless, the Gilbert damping constant remains nearly unchanged after annealing. The PMA also increases with the thickness of W insertion layer. Both acoustic (in-phase) mode and optical (out-of-phase) mode are observed. The optical mode, which is typically weak when using the conventional FMR measurement, shows a comparable magnitude to the acoustic mode. The effective excitation of optical mode is ascribed to the non-uniform spin-orbit torque acting on the two coupled layers. Furthermore, the interlayer exchange coupling (ferromagnetic or antiferromagnetic) can be identified through analyzing the two resonance modes, which is found to depend on the W insertion layer thickness, CoFeB layer thickness, and annealing conditions. The experimental results will be useful for developing high-frequency magnetic devices based on magnetic multilayer films with high PMA and thermal stability. Our experimental results also show that the ST-FMR is an effective methodology for studying interlayer exchange coupled systems.

## I . INTRODUCTION

Magnetic tunnel junctions (MTJs) with a perpendicular magnetic anisotropy (PMA) have attracted tremendous attentions for their potentials in developing high density, high thermal stability, and low-power consumption spin-transfer torque (STT)/spin-orbit torque (SOT) magnetic random-access memory (MRAM).[1-6] Among the available PMA systems that are compatible with MTJs, the heavy metal/CoFeB/MgO system has demonstrated the capability of facilitating a high tunneling magnetoresistance (TMR) ratio and the compatibility with complementary metal-oxide-semiconductor (CMOS) technology.[3, 7, 8] Moreover, this structure allows the SOT-driven magnetization switching, offering advantages over conventional STT in terms of power consumption and the fact that the high write current does not pass through the tunnel barrier of the MTJ.[3, 9]

To increase data retention time, a strong PMA is required. In the heavy metal/CoFeB/MgO films, the PMA mainly originates from the interfacial PMA at the CoFeB/MgO interface.[3] Nevertheless, the heavy metal/CoFeB interface also plays an important role in achieving high PMA.[10] It has been found that the PMA can be increased by inserting ultrathin metals in the CoFeB layer.[11-16] Very recently, a high PMA has been reported in the MgO/CoFeB/W(insertion)/CoFeB/W (from bottom to top) and MgO/CoFeB/W(insertion)/CoFeB/MgO stacks,[17, 18] which also show high thermal stability, making them more promising for practical applications. The former structure is of particular interest because the top W layer with large spin Hall angle allows energy-efficient manipulation of the perpendicular magnetization

using in-plane current-induced SOTs.[4, 19] However, it is still unclear how the thicknesses of CoFeB and W insertion layers affect the PMA as well as other magnetic characteristics, such as the resonance frequency and field, Gilbert damping constant ( $\alpha$ ), and interlayer coupling modes. Understanding all of these properties can help improve the contribution/role of the materials towards practical applications.

In this work, we study the ferromagnetic resonance properties of the W/CoFeB/W(insertion)/CoFeB/MgO (from bottom to top) structures using the spin-torque ferromagnetic resonance (ST-FMR) technique.[20-22] The thicknesses of CoFeB and W insertion layers are systematically adjusted to explore their effects on the PMA. More importantly, the influence of annealing, CoFeB layer thickness, and W insertion layer thickness on the magnetic damping constants and interlayer exchange coupling can be identified by analyzing the ST-FMR spectra. These results may be useful for developing high-frequency magnetic devices based on magnetic multilayer films with high PMA and thermal stability.

## II. SAMPLE PREPARATION AND ST-FMR MEASUREMENT

The stacks consisting of W(5)/CoFeB( $t_1$ )/W( $t$ )/CoFeB( $t_2$ )/MgO(2)/Ta(2) ( $t_1 = t_2$ , thicknesses are in nm) were deposited on thermally oxidized Si (001) substrates by magnetron sputtering system at room temperature. The two CoFeB layers were grown in a wedge shape with the thicknesses varying from 0.69 nm to 1.31 nm, as shown in Fig. 1(a). Subsequently, the multilayer stacks were patterned into rectangular-shaped strips (length of 20  $\mu\text{m}$  and width of 20  $\mu\text{m}$ ) using optical lithography and dry etching. Cr(10)/Au(100) metal stacks were deposited as electrodes for electrical

measurements. The annealing treatment was carried out at 400 °C for 0.5 hour in a vacuum environment without an external magnetic field. Figure 1(b) shows the schematic diagram of the ST-FMR measurement setup. A microwave current  $I_{c,rf}$  with a power of 6 dBm is applied to the device to generate a microwave-frequency SOT on the ferromagnetic layers, which oscillates the magnetization, resulting in an oscillation of the longitudinal resistance due to spin hall magnetoresistance (SMR) effect. A rectified voltage  $V_{mix}$  due to the mixing of rf current and the time-varying resistance was detected by using a lock-in amplifier. An in-plane magnetic field with a fixed angle  $\theta_H$  of 45° was swept between -0.5 T and +0.5 T, where  $\theta_H$  is the angle between the external field and the current channel. All the measurements were carried out at room temperature.

### III. EXPERIMENTAL RESULTS AND DISCUSSION

#### A. ST-FMR SPECTRA OF THE MAGNETIC MULTILAYER STACKS

Figure 1(c) shows the typical ST-FMR spectra for the as-grown sample with CoFeB layers of  $t_1 + t_2 = 1.95$  nm and a W insertion layer of 0.4 nm. The spectrum can be well fitted to the sum of a symmetric and an antisymmetric Lorentzian functions[23],

$$V_{mix} = S \frac{\Delta^2}{\Delta^2 + (\mu_0 H_{ext} - \mu_0 H_0)^2} + A \frac{\Delta(\mu_0 H_{ext} - \mu_0 H_0)}{\Delta^2 + (\mu_0 H_{ext} - \mu_0 H_0)^2} \quad (1)$$

which mainly originates from the damping-like SOT, and field-like SOT as well as Oersted field torque, respectively[24].  $\Delta$  is the linewidth (full width at half maximum),  $\mu_0 H_0$  is the resonant magnetic field,  $\mu_0 H_{ext}$  is the applied magnetic field,  $S$  is the symmetric Lorentzian coefficient that is proportional to the oscillating spin current  $I_{s,rf}$ ,

and  $A$  is the antisymmetric Lorentzian coefficient that is proportional to the Oersted field  $\mu_0 H_{rf}$  generated by  $I_{rf}$ . One single resonance peak is observed for a given frequency, and the resonance magnetic field increases with the frequency, which is a typical signature resulting from the in-plane magnetic anisotropy. Figure 1(d) shows a ST-FMR spectrum for the annealed sample. In contrast to the spectra for the as-grown samples (Fig. 1(c)), two resonance peaks are observed for the annealed samples, which is a signature of PMA[22]. The two peaks can be separately fitted using Equation 1. The linewidth  $\Delta$  and resonant magnetic field  $\mu_0 H_0$  are thus extracted, and used for analyzing the magnetic anisotropy and damping constant as discussed in the following sections.

## B. THE EFFECTIVE MAGNETIZATION FIELDS AND GILBERT DAMPING

Figure 2(a) shows the resonance frequency  $f$  as a function of resonant field  $\mu_0 H_0$  for as-grown samples with different CoFeB thicknesses and a 0.4 nm-thick W insertion layer. The effective magnetization fields  $4\pi M_{eff}$  are extracted from the Kittel equation fitting[19, 23, 25],

$$f = (\gamma/2\pi)[\mu_0 H_0(\mu_0 H_0 + 4\pi M_{eff})]^{1/2} \quad (2)$$

where  $\gamma$  is the gyromagnetic ratio. Figure 2(b) shows the dependences of resonance frequency  $f$  on the resonant field  $\mu_0 H_0$  for the annealed samples. Compared with the results for as-grown samples, the most striking feature for the annealed samples is the emergence of an additional branch at low-field region as the thicknesses of CoFeB layers decrease (e.g.,  $t_1 + t_2 = 1.88$  nm). This additional branch corresponds to the additional resonance peak at low-field region for the perpendicularly magnetized

samples, as shown in Fig. 1(d). For the samples with a PMA, the magnetization is not aligned with the external magnetic field as the magnitudes of the field are below the alignment field  $\mu_0 H_a^{FMR}$ . For the right branch,  $H_0 > H_a^{FMR}$ , the resonant frequency dependence on magnetic field can still be fitted by Kittel equation approximately. For  $H_0 < H_a^{FMR}$ , the left branch can be described by the following equation,

$$f = (\gamma/2\pi)[(\mu_0 H_k)^2 - (\mu_0 H_0)^2]^{1/2} \quad (0 < H_0 < H_k) \quad (3)$$

which was derived from the previous work[26]. Here,  $\mu_0 H_k = \mu_0 H_\perp - 4\pi M_S = -4\pi M_{eff}$ .

Figure 3(a) shows the extracted effective magnetization fields as a function of CoFeB layer thickness for the samples with W insertion layer thicknesses of 0.2 nm (red circle) and 0.4 nm (blue hexagon). The results for the sample with single layer CoFeB (reported in the Ref. 21), i.e. without a W insertion layer, are also shown in the figure for comparison (black square). The values of  $4\pi M_{eff}$  are positive for all the as-grown samples, implying an in-plane magnetic anisotropy. For a given CoFeB layer thickness,  $4\pi M_{eff}$  decreases after inserting a W layer, reflecting the enhancement of PMA. Since the PMA also originates from the interface between CoFeB and heavy metal, such an enhancement is ascribed to the additional CoFeB/W interfaces[10, 17, 18]. Furthermore, compared with the PMA for the sample with a 0.2 nm-thick W insertion layer, the enhancement for the 0.4 nm case is more pronounced. This again reflects the importance of high-quality interfaces because the 0.4 nm-thick W insertion layer has better continuity and uniformity compared to the 0.2 nm-thick one. After annealing the samples,  $4\pi M_{eff}$  becomes negative for the samples with relatively

thin CoFeB layers, indicating that the anisotropy field of the system changes from in-plane to out-of-plane. The samples with W insertion layers have a more pronounced increase of PMA compared with those without W insertion, again indicating that the W/CoFeB interface helps to enhance the PMA<sup>10</sup>.

The frequency dependences of resonance linewidths are summarized in Fig. 2(c). The resonance linewidth can be fitted by[19, 25]:

$$\Delta = \Delta_0 + (2\pi\alpha/\gamma)f \quad (4)$$

where  $\Delta_0$  is the extrinsic contribution (*e.g.*, inhomogeneous broadening) to the linewidth, which is usually independent of frequency. The second term is the intrinsic contribution (*e.g.*, Gilbert damping), which is linearly proportional to frequency. The  $\alpha$  values for the samples with 0.2 nm- and 0.4 nm-thick W insertion layers as a function of CoFeB thickness are then extracted and shown in Fig. 3(b). The as-grown and annealed samples with 0.2 nm-thick W insertion layers show comparable  $\alpha$  values and similar dependences on the CoFeB layer thickness to the sample without an insertion layer. While, increasing the W insertion layer thickness leads to the increase of  $\alpha$  for a given CoFeB thickness. We also notice that, different from the as-grown samples,  $\alpha$  does not increase monotonously as the thickness of CoFeB stacks decreases in the annealed samples with W insertion layer. Instead,  $\alpha$  first increases along with the decrease of the CoFeB thickness, but then decreases abruptly at some critical CoFeB thickness. That may be related to the increased interfacial PMA, which requires further investigation.

### C. THE EXCHANGE COUPLING BETWEEN THE COFEB LAYERS

Figures 4(a) and (b) show the ST-FMR spectra (13 GHz) for the as-grown and annealed samples with CoFeB layer thicknesses of  $t_1 + t_2 = 2.37$  nm and a 0.6 nm-thick W insertion layer. Strikingly, two peaks are observed in ST-FMR spectra for both as-grown and annealed samples of  $t_1 + t_2 > 2.0$  nm, as shown by the green and blue fitting curves. Notably, the linewidth of the green one is much narrower than that of the blue one, for both the as-grown and annealed samples, as shown in the Figs. 4(c) and (d). Interestingly, the resonance field of the narrower linewidth is lower than that of the wider one for the as-grown sample, as shown in Fig. 4(a), while the resonance field of the narrower one becomes larger than that of the wider one after annealing, as shown in Figs. 4(b). Such a feature is visible for all the measured frequency range, as shown in Figs. 4(e) and (f). We point out that these two peaks have different origins compared to those of the samples with PMA. First of all, the dependence of resonant frequency on the resonant field for both the narrower and wider peaks follows the Kittel equation, indicating that the film exhibits an in-plane magnetic anisotropy. The in-plane magnetic anisotropy is further verified by the extracted positive values of  $4\pi M_{\text{eff}}$  for the as-grown and annealed samples (see Fig. 5(a)) and by magneto-optical Kerr effect (MOKE) measurement (to be discussed later).

We attribute the observation of two resonance peaks to the emergence of two different modes of the ferromagnetic resonance of the CoFeB/W/CoFeB layers. In addition to the in-phase resonance, the weak coupling between the two CoFeB layers can also lead to an out-of-phase resonance. These two modes had been previously observed in NiFe/Ru/NiFe and Fe/[Co/Cu]<sub>10</sub>/Co/Pt structures.[27-30] The in-phase

and out-of-phase resonances are referred to as acoustic (symmetric) mode and the optical (antisymmetric) mode, respectively. Another pronounced feature observed in the previous experiments is that the linewidths (as well as the Gilbert damping) of the optical modes are greater than those of the acoustic modes[27, 28, 31], which are consistently shown by our results (see Fig. 5(b)). The damping constants of the acoustic modes remain relatively low, while those of the optical modes increase (for  $t_1 + t_2 > 2.0$  nm). This could be qualitatively explained by the framework of the mutual spin pumping effect.[27, 31] In the out-of-phase precession, the pumped spin accumulation and spin current are greatly amplified compared to those of the in-phase precession mode, resulting in a giant enhancement of the Gilbert damping in the out-of-phase precession mode.[27, 29, 31]

The resonance fields of the acoustic ( $\mu_0 H_0^S$ ) and optical ( $\mu_0 H_0^A$ ) modes can be described by[29]:

$$\mu_0 H_0^A = \mu_0 H_0^S + 2\mu_0 H_{ex} \quad \mu_0 H_{ex} = -A_{ex}/M_S t_F \quad (5)$$

where  $A_{ex}$  is the strength of the exchange coupling and  $t_F$  is thickness of ferromagnetic layer ( $t_F = t_1 = t_2$ ). A positive  $A_{ex}$  corresponds to ferromagnetic (FM) coupling and a negative one corresponds to antiferromagnetic (AFM) coupling[28]. Therefore, the optical mode has the lower resonance field in the FM coupled system, while it has a higher resonance field in the AFM coupled system. We are able to extract the coupling fields  $\mu_0 H_{ex}$  by directly measuring the difference between the acoustic and optical mode resonance fields, as shown in Fig. 6(a). The exchange coupling strengths  $A_{ex}$  are therefore extracted through Equation (5) using  $M_s$

= 1.008 MA/m reported by our previous work.[22]  $A_{ex}$  is negative for the as-grown samples, indicating an AFM coupling between the two CoFeB layers. However, for the annealed sample,  $A_{ex}$  turns to be positive, indicating an FM coupling between the two CoFeB layers. We point out that, for  $t_1 + t_2 < 2.0$  nm, only one resonance peak is observed. This implies that the two CoFeB layers are strongly coupled with each other, similar to a single layer of CoFeB. These results indicate that the coupling between the two CoFeB layers is not only dependent on the W insertion layer thickness, but also on the CoFeB layer thickness.

To further verify the obtained coupling types in as-grown and annealed samples, magnetic hysteresis loops are measured by MOKE, as shown in Fig. 6(b). In the upper panel, the hysteresis loop of the as-grown sample with  $t_1 + t_2 = 2.55$  nm shows an AFM coupling[16, 32, 33]. However, after annealing, this sample changes to show FM coupling (the middle panel). In the lower panel, the hysteresis loop of the as-grown sample with CoFeB layer thickness of  $t_1 + t_2 = 1.56$  nm shows an FM exchange coupling. The results of the MOKE measurements confirm our inference from ST-FMR spectra analysis.

It is known that the two ferromagnetic layers that are separated by a nonmagnetic metal can be indirectly coupled through the Ruderman-Kittel-Kasuya-Yosida (RKKY) interaction[34-36]. The coupling can be either ferromagnetic or antiferromagnetic, depending on the sign of the coupling coefficient  $J_{ij}^{RKKY}$ , which shows an oscillatory behavior as a function of the thickness of the spacer layer[35-38]. For the samples with insertion layer of 0.6 nm, the two CoFeB layers with  $t_1 + t_2 > 2.0$  nm are likely

coupled through indirect RKKY interaction in an antiferromagnetic manner. After annealing, the exchange coupling in the sample with 0.6 nm-thick W insertion layer changes from AFM to FM correspondingly, as shown in the upper and middle panels of Fig. 6(b). We believe this transition is related to the inter-diffusion among the layers promoted by the annealing process, which is revealed by the transmission electron microscopy measurement. Figure 7a shows the samples structure of the studied sample. The inter-diffusion between W and CoFeB layers can be proved by the line profiles for individual elements as shown in Figs. 7(b) and (c), which were extracted from the high-angle annular dark-field images with line scan-energy dispersive spectra. We speculate that the inter-diffusion changes the effective W layer thickness, which changes the coupling coefficient  $J_{ij}^{RKKY}$ . It is noted that the orange-peel coupling can also result in parallel or antiparallel interlayer coupling for perpendicular magnetization due to the relatively large surface roughness ( $\sim 12$  Å)[39]. In our multilayers, the surface roughness is  $< 5$  Å based on TEM image, and thus, we speculate that the orange-peel coupling plays a minor role.

It would be counterintuitive to conclude that the coupling type varies with the CoFeB layer thickness. This may imply that the morphology of the insertion layer also depends on the CoFeB thickness. For the samples with CoFeB stacks thinner than 2.0 nm, the surface morphology may not allow for the growth of a continuous W layer, as shown in the inset of the lower panel of Fig. 6(b). Similar to this situation, for the samples with 0.2 nm- and 0.4 nm-thick W insertion layers, the W insertion layer may be too thin to be continuous as well. As a result, the CoFeB layers cannot be well

separated, resulting in a direct exchange coupling.

Our results indicate that the ST-FMR can be used to excite and identify the acoustic and optical resonance modes of interlayer exchange coupled ferromagnetic layers, which are typically accomplished by FMR technique. In addition to providing an alternative technique, there is an extra advantage of using ST-FMR. For conventional FMR technique, the signal magnitude of excited optical mode is typically much smaller than the acoustic mode because the out-of-phase resonance cannot efficiently couple to a uniform excitation magnetic field over the sample[30, 40], especially for two identical ferromagnetic layers. This problem can be overcome via using a ST-FMR technique. Different from the uniform magnetic field excitation, the SOT is not uniformly applied to the two ferromagnetic layers. In the studied sample, the SOT is mainly applied to the CoFeB layer that is adjacent to the bottom W layer. This is because the spin current generated from the W layer is mainly absorbed by the adjacent CoFeB layer and barely diffuse into the second CoFeB layer. As a result, the excitation of optical mode is more efficient and the magnitude is pronounced in our experiment.

#### IV. CONCLUSION

We investigate the magnetic properties of both the as-grown and annealed W/CoFeB/W/CoFeB/MgO stacks with different thicknesses of the CoFeB and W insertion layers using ST-FMR technique. By analyzing the ST-FMR spectra, we systematically studied the dependences of the magnetic anisotropy, damping constant, and interlayer exchange coupling on the effects of annealing, CoFeB layer thicknesses,

and W insertion layer thicknesses. It was found that the PMA is strongly enhanced after annealing, while the Gilbert damping constant remains nearly unchanged. The PMA also increases with increasing the thickness of W insertion layer. The direct exchange coupling or indirect RKKY interaction between the two CoFeB layers can also be identified using ST-FMR technique, which is found to depend on the W insertion layer thickness, CoFeB layer thickness, and annealing conditions. Our results indicate that the ST-FMR measurement is also an effective methodology in probing the interlayer exchange coupling between magnetic multilayers. Our present work will be useful for designing and developing magnetic devices using the W-based structures with large PMA and high thermal stability.

#### **ACKNOWLEDGEMENTS**

This work was supported by the financial support from the National Natural Science Foundation of China [NSFC, Grants No.11874409], National Natural Science Foundation of China (NSFC)-Science Foundation Ireland (SFI) Partnership Programme [Grant No. 51861135104], and 1000 Youth Talents Program. This work was also supported in part by C-SPIN and FAME, two of six centers of STARnet, a Semiconductor Research Corporation program, sponsored by MARCO and DARPA. This work was also supported by the National Science Foundation (ECCS 1611570) and Nanosystems Engineering Research Center for Translational Applications of Nanoscale Multiferroic Systems (TANMS) Cooperative Agreement Award EEC-1160504.

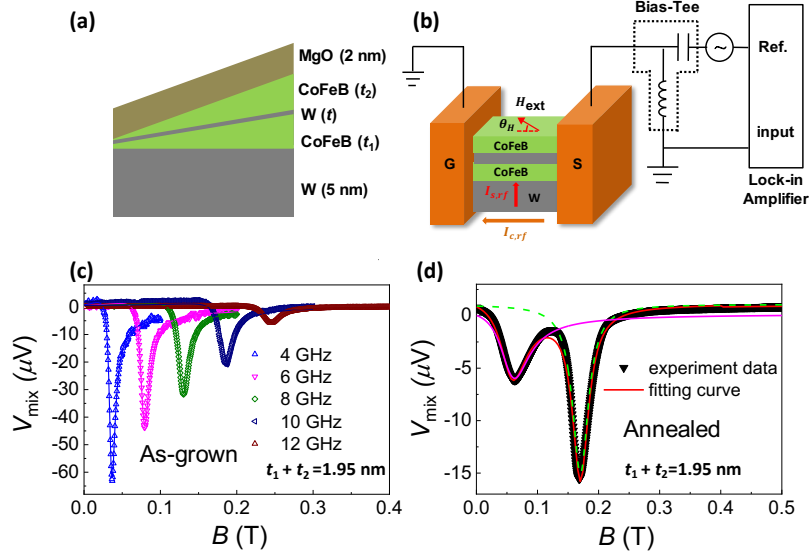


Fig. 1 (a) The schematic diagram of the magnetic multilayer stack with a W insertion layer. (b) The schematic diagram of ST-FMR measurement setup. The charge current  $I_{c,rf}$  is marked by orange arrow, and the spin current  $I_{s,rf}$  is indicated by red arrow.  $H_{ext}$  is the applied external magnetic field.  $\theta_H$  is the angle between  $H_{ext}$  and the current channel. (c) The ST-FMR spectra for the as-grown sample with CoFeB layers of  $t_1 + t_2 = 1.95$  nm and a W insertion layer of 0.4 nm. The solid curves are the fits to a sum of symmetric and antisymmetric Lorentzian functions. (d) The ST-FMR spectrum for the annealed sample under frequency of 3.0 GHz. The same device is measured to obtain the results before (c) and after (d) annealing. Two resonance peaks were observed, which is a signature of PMA.

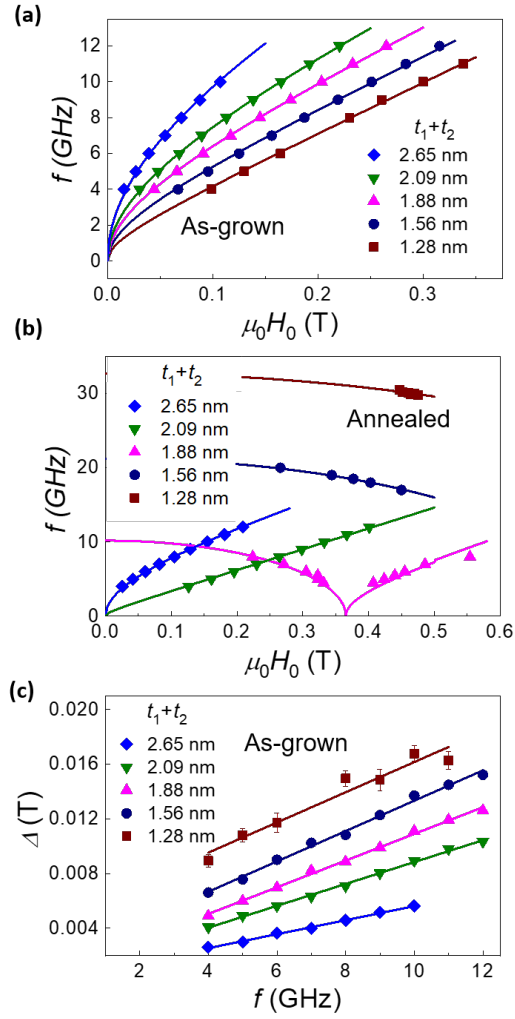


Fig. 2 Resonance frequency  $f$  as a function of the resonant field  $\mu_0 H_0$  for the as-grown (a) and annealed (b) samples with different CoFeB layer thicknesses. The W insertion layer thickness is 0.4 nm. The solid lines are fitting curves. For the annealed sample (e.g.,  $t_1 + t_2 = 1.88$  nm), the resonance frequency dependence on the resonant field exhibits an additional branch as the thickness of the CoFeB stacks decrease. (c) The linewidth  $\Delta$  extracted from the fitting of ST-FMR spectra versus the resonance frequency  $f$  for different CoFeB layer thicknesses. The lines are linear fittings.

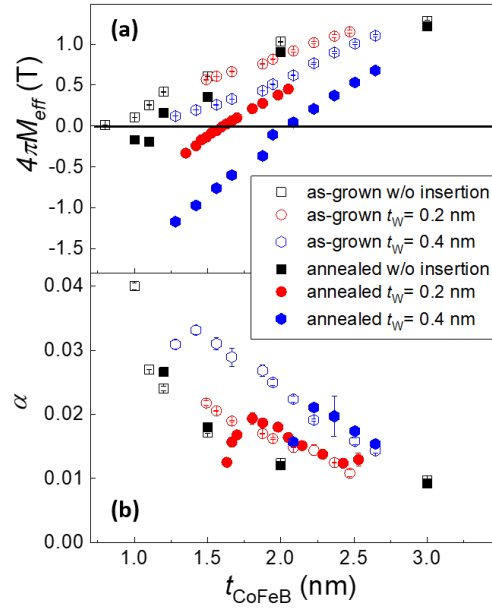


Fig. 3 (a) The effective magnetization fields,  $4\pi M_{\text{eff}}$ , as a function of CoFeB thickness for the as-grown and annealed samples with and without (reported in the Ref. 21) W insertion layers. (b) The Gilbert damping constant  $\alpha$ , for the as-grown and annealed samples, extracted from the linear fitting of the linewidth versus the frequency  $f$ .

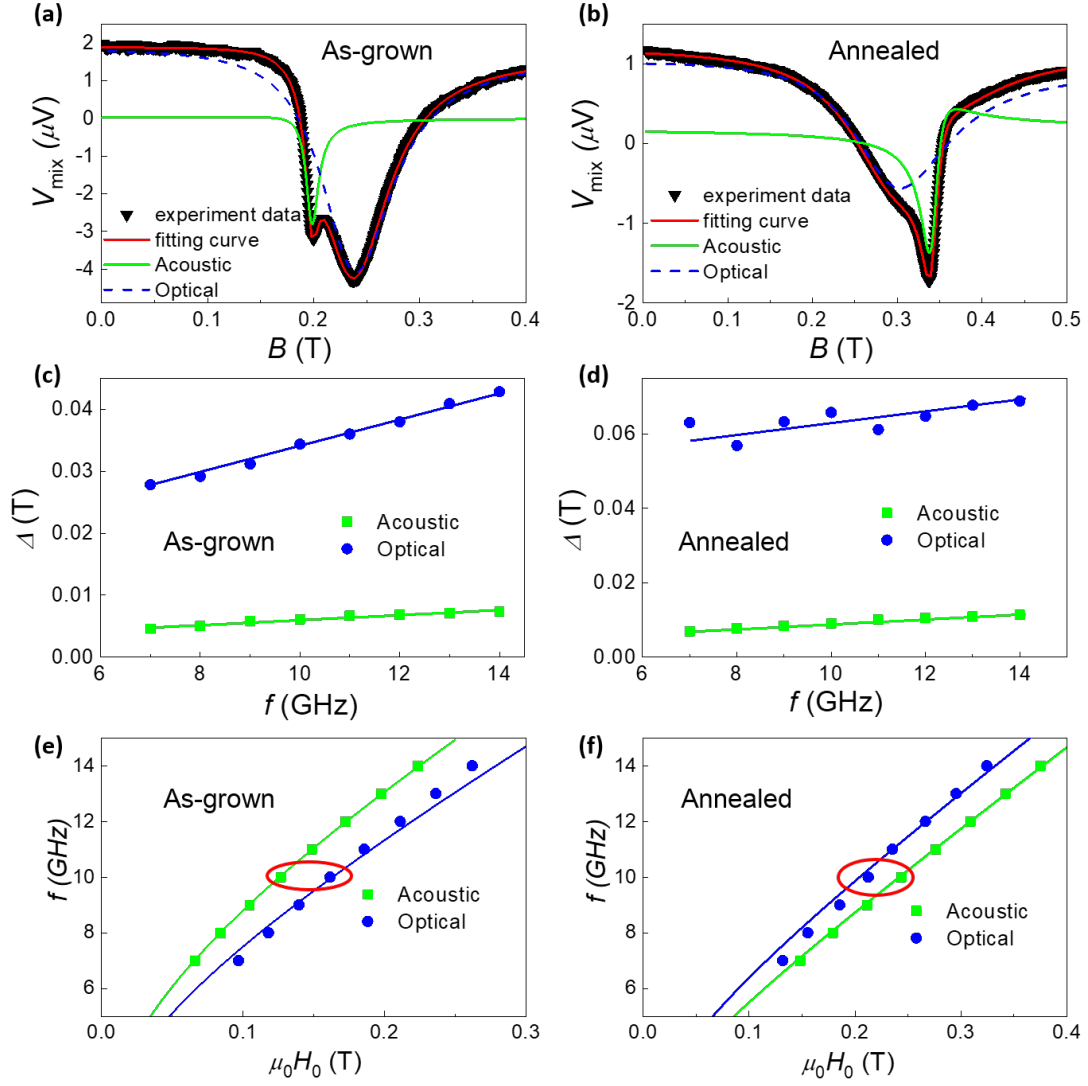


Fig. 4 The ST-FMR spectra (13 GHz) for the as-grown (a) and annealed (b) samples with CoFeB layer thicknesses of  $t_1 + t_2 = 2.37$  nm and a 0.6 nm-thick W insertion layer. Two peaks are observed in both ST-FMR spectra, which are attributed to the symmetric (acoustic) and antisymmetric (optical) modes. The fitting curves are indicated by the lines. The linewidth  $\Delta$  as a function of the resonance frequency  $f$  for the as-grown (c) and annealed (d) samples. Resonance frequency  $f$  as a function of the resonant field  $\mu_0 H_0$  for the two different modes, in as-grown (e) and annealed (f) samples. The solid curves are fittings by Kittel equation.

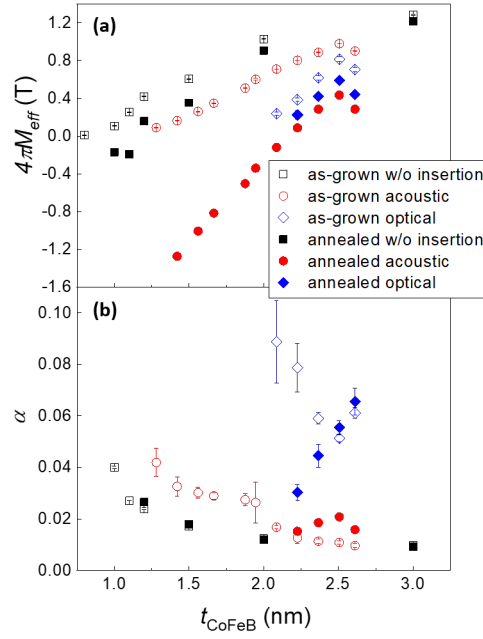


Fig. 5 (a) The effective magnetization fields ( $4\pi M_{\text{eff}}$ ) and (b) the Gilbert damping constant  $\alpha$  for the as-grown and annealed samples with and without a W insertion layer as a function of CoFeB thickness. The W insertion layer thickness is 0.6 nm.

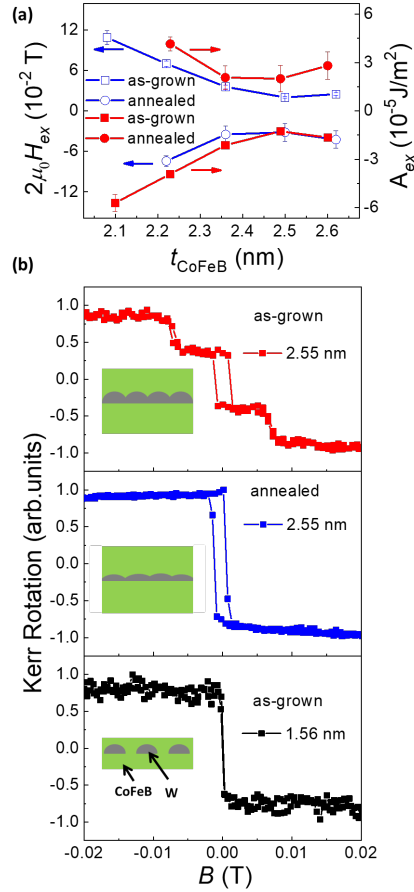


Fig. 6 (a) The interlayer exchange coupling extracted from the resonance field shift of the acoustic and optical modes ( $t_{\text{CoFeB}} = t_1 + t_2$ ).  $A_{\text{ex}}$  is negative for the as-grown samples, corresponding to an antiferromagnetic coupling. However, for the annealed samples,  $A_{\text{ex}}$  becomes positive, corresponding to a ferromagnetic coupling. (b) In-plane magnetic hysteresis loops for the as-grown and annealed CoFeB stacks. The upper panel: The hysteresis loop shows antiferromagnetic coupling (as-grown,  $t_1 + t_2 = 2.55 \text{ nm}$ ). The middle panel: The hysteresis loop shows ferromagnetic coupling (annealed,  $t_1 + t_2 = 2.55 \text{ nm}$ ). The lower panel: The hysteresis loop shows ferromagnetic exchange coupling (as-grown,  $t_1 + t_2 = 1.56 \text{ nm}$ ). The insets are the corresponding CoFeB/W/CoFeB film structures.

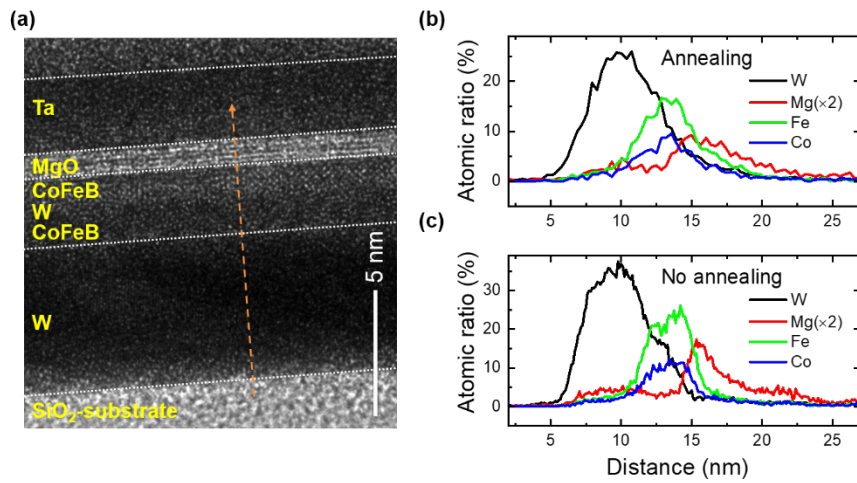


Fig. 7(a). The high-resolution TEM image of as-grown W(5)/CoFeB(1.28)/W(0.6)/CoFeB(1.28)/MgO(2)/Ta(2) (units in nm), (b) and (c) the line profiles (along the orange dashed line direction in (a)) for individual elements extracted from the high-angle annular dark-field images with line scan-energy dispersive spectra for the annealed and non-annealed samples, respectively.

- [1] Mangin, S., D. Ravelosona, J.A. Katine, M.J. Carey, B.D. Terris, and E.E. Fullerton, Current-induced magnetization reversal in nanopillars with perpendicular anisotropy, *Nat. Mater.* 5, 210 (2006).
- [2] Kishi, T., H. Yoda, T. Kai, T. Nagase, E. Kitagawa, M. Yoshikawa, K. Nishiyama, T. Daibou, M. Nagamine, M. Amano, S. Takahashi, M. Nakayama, N. Shimomura, H. Aikawa, S. Ikegawa, S. Yuasa, K. Yakushiji, H. Kubota, A. Fukushima, M. Oogane, T. Miyazaki, and K. Ando. *Lower-current and fast switching of a perpendicular TMR for high speed and high density spin-transfer-torque MRAM. 2008 IEEE International Electron Devices Meeting. 2008.*
- [3] Ikeda, S., K. Miura, H. Yamamoto, K. Mizunuma, H.D. Gan, M. Endo, S. Kanai, J. Hayakawa, F. Matsukura, and H. Ohno, A perpendicular-anisotropy CoFeB-MgO magnetic tunnel junction, *Nat. Mater.* 9, 721 (2010).
- [4] Miron, I.M., K. Garello, G. Gaudin, P.-J. Zermatten, M.V. Costache, S. Auffret, S. Bandiera, B. Rodmacq, A. Schuhl, and P. Gambardella, Perpendicular switching of a single ferromagnetic layer induced by in-plane current injection, *Nature* 476, 189 (2011).
- [5] Liu, L., O.J. Lee, T.J. Gudmundsen, D.C. Ralph, and R.A. Buhrman, Current-Induced Switching of Perpendicularly Magnetized Magnetic Layers Using Spin Torque from the Spin Hall Effect, *Phys. Rev. Lett.* 109, 096602 (2012).
- [6] Yu, G.Q., P. Upadhyaya, Y.B. Fan, J.G. Alzate, W.J. Jiang, K.L. Wong, S. Takei, S.A. Bender, L.T. Chang, Y. Jiang, M.R. Lang, J.S. Tang, Y. Wang, Y. Tserkovnyak, P.K. Amiri, and K.L. Wang, Switching of perpendicular magnetization by spin-orbit torques in the absence of external magnetic fields, *Nat. Nanotechnol.* 9, 548 (2014).
- [7] Yoda, H., T. Kishi, T. Nagase, M. Yoshikawa, K. Nishiyama, E. Kitagawa, T. Daibou, M. Amano, N. Shimomura, S. Takahashi, T. Kai, M. Nakayama, H. Aikawa, S. Ikegawa, M. Nagamine, J. Ozeki, S. Mizukami, M. Oogane, Y. Ando, S. Yuasa, K. Yakushiji, H. Kubota, Y. Suzuki, Y. Nakatani, T. Miyazaki, and K. Ando, High efficient spin transfer torque writing on perpendicular magnetic tunnel junctions for high density MRAMs, *Curr. Appl. Phys.* 10, E87 (2010).
- [8] Endo, M., S. Kanai, S. Ikeda, F. Matsukura, and H. Ohno, Electric-field effects on thickness dependent magnetic anisotropy of sputtered MgO/Co<sub>40</sub>Fe<sub>40</sub>B<sub>20</sub>/Ta structures, *Appl. Phys. Lett.* 96, 212503 (2010).
- [9] Wang, K.L., J.G. Alzate, and P.K. Amiri, Low-power non-volatile spintronic memory: STT-RAM and beyond, *J. Phy. D: Appl. Phys.* 46, 074003 (2013).
- [10] Worledge, D.C., G. Hu, D.W. Abraham, J.Z. Sun, P.L. Trouilloud, J. Nowak, S. Brown, M.C. Gaidis, E.J. O' Sullivan, and R.P. Robertazzi, Spin torque switching of perpendicular Ta | CoFeB | MgO-based magnetic tunnel junctions, *Appl. Phys. Lett.* 98, 022501 (2011).
- [11] Naik, V.B., H. Meng, and R. Sbiaa, Thick CoFeB with perpendicular magnetic anisotropy in CoFeB-MgO based magnetic tunnel junction, *AIP Adv.* 2, 042182 (2012).
- [12] Sato, H., M. Yamanouchi, S. Ikeda, S. Fukami, F. Matsukura, and H. Ohno, Perpendicular-anisotropy CoFeB-MgO magnetic tunnel junctions with a MgO/CoFeB/Ta/CoFeB/MgO recording structure, *Appl. Phys. Lett.* 101, 022414 (2012).
- [13] Sato, H., E.C.I. Enobio, M. Yamanouchi, S. Ikeda, S. Fukami, S. Kanai, F. Matsukura, and H. Ohno, Properties of magnetic tunnel junctions with a MgO/CoFeB/Ta/CoFeB/MgO recording structure down to junction diameter of 11 nm, *Appl. Phys. Lett.* 105, 062403 (2014).
- [14] Huang, T., X. Cheng, X. Guan, and X. Miao, Effect of Ultrathin Inserted Ag Layer on Perpendicular Magnetic Anisotropy of CoFeB Thin Film, *IEEE Trans. Magn.* 50, 1 (2014).

- [15] Cuchet, L., B. Rodmacq, S. Auffret, R.C. Sousa, I.L. Prejbeanu, and B. Dieny, Perpendicular magnetic tunnel junctions with double barrier and single or synthetic antiferromagnetic storage layer, *J. Appl. Phys.* 117, 233901 (2015).
- [16] Zhang, X., Y. Zhang, and J.W. Cai, Antiferromagnetically coupled perpendicular magnetic anisotropic CoFeB/MgO films across a Mo spacer with high thermal stability, *J. Appl. Phys.* 118, 143903 (2015).
- [17] Kim, J.-H., J.-B. Lee, G.-G. An, S.-M. Yang, W.-S. Chung, H.-S. Park, and J.-P. Hong, Ultrathin W space layer-enabled thermal stability enhancement in a perpendicular MgO/CoFeB/W/CoFeB/MgO recording frame, *Sci. Rep.* 5, 16903 (2015).
- [18] Liu, Y., T. Yu, Z.Y. Zhu, H.C. Zhong, K.M. Khamis, and K.G. Zhu, High thermal stability in W/MgO/CoFeB/W/CoFeB/W stacks via ultrathin W insertion with perpendicular magnetic anisotropy, *J. Magn. Magn. Mater.* 410, 123 (2016).
- [19] Pai, C.-F., L. Liu, Y. Li, H.W. Tseng, D.C. Ralph, and R.A. Buhrman, Spin transfer torque devices utilizing the giant spin Hall effect of tungsten, *Appl. Phys. Lett.* 101, 122404 (2012).
- [20] Cho, S., S.H.C. Baek, K.D. Lee, Y. Jo, and B.G. Park, Large spin Hall magnetoresistance and its correlation to the spin-orbit torque in W/CoFeB/MgO structures, *Sci. Rep.* 5, 14668 (2015).
- [21] Kim, J., P. Sheng, S. Takahashi, S. Mitani, and M. Hayashi, Spin Hall Magnetoresistance in Metallic Bilayers, *Phys. Rev. Lett.* 116, 097201 (2016).
- [22] He, C., A. Navabi, Q. Shao, G. Yu, D. Wu, W. Zhu, C. Zheng, X. Li, Q.L. He, S.A. Razavi, K.L. Wong, Z. Zhang, P.K. Amiri, and K.L. Wang, Spin-torque ferromagnetic resonance measurements utilizing spin Hall magnetoresistance in W/Co<sub>40</sub>Fe<sub>40</sub>B<sub>20</sub>/MgO structures, *Appl. Phys. Lett.* 109, 202404 (2016).
- [23] Liu, L.Q., T. Moriyama, D.C. Ralph, and R.A. Buhrman, Spin-Torque Ferromagnetic Resonance Induced by the Spin Hall Effect, *Phys. Rev. Lett.* 106, 036601 (2011).
- [24] Mellnik, A.R., J.S. Lee, A. Richardella, J.L. Grab, P.J. Mintun, M.H. Fischer, A. Vaezi, A. Manchon, E.A. Kim, N. Samarth, and D.C. Ralph, Spin-transfer torque generated by a topological insulator, *Nature* 511, 449 (2014).
- [25] Nan, T.X., S. Emori, C.T. Boone, X.J. Wang, T.M. Oxholm, J.G. Jones, B.M. Howe, G.J. Brown, and N.X. Sun, Comparison of spin-orbit torques and spin pumping across NiFe/Pt and NiFe/Cu/Pt interfaces, *Phys. Rev. B* 91, 214416 (2015).
- [26] Mizukami, S., Y. Ando, and T. Miyazaki, The study on ferromagnetic resonance linewidth for NM/80NiFe/NM (NM = Cu, Ta, Pd and Pt) films, *Japan. J. Appl. Phys.* 40, 580 (2001).
- [27] Kensho, T., M. Takahiro, N. Masaki, S. Takeshi, T. Koki, T. Saburo, and O. Teruo, Linewidth broadening of optical precession mode in synthetic antiferromagnet, *Appl. Phys. Express* 7, 063010 (2014).
- [28] Belmeguenai, M., T. Martin, G. Woltersdorf, M. Maier, and G. Bayreuther, Frequency- and time-domain investigation of the dynamic properties of interlayer-exchange-coupled Ni<sub>81</sub>Fe<sub>19</sub> / Ru / Ni<sub>81</sub>Fe<sub>19</sub> thin films, *Phys. Rev. B* 76, 104414 (2007).
- [29] Yang, H., Y. Li, and W.E. Bailey, Large spin pumping effect in antisymmetric precession of Ni<sub>79</sub>Fe<sub>21</sub>/Ru/Ni<sub>79</sub>Fe<sub>21</sub>, *Appl. Phys. Lett.* 108, 242404 (2016).
- [30] Heinrich, B., J.F. Cochran, M. Kowalewski, J. Kirschner, Z. Celinski, A.S. Arrott, and K. Myrtle, Magnetic anisotropies and exchange coupling in ultrathin fcc Co(001) structures, *Phys. Rev. B* 44, 9348 (1991).
- [31] Takahashi, S., Giant enhancement of spin pumping in the out-of-phase precession mode, *Appl.*

- Phys. Lett. 104, 052407 (2014).
- [32] Wiese, N., T. Dimopoulos, M. Ruhrig, J. Wecker, H. Bruckl, and G. Reiss, Antiferromagnetically coupled CoFeB/Ru/CoFeB trilayers, *Appl. Phys. Lett.* 85, 2020 (2004).
- [33] Lee, J.-B., G.-G. An, S.-M. Yang, H.-S. Park, W.-S. Chung, and J.-P. Hong, Thermally robust perpendicular Co/Pd-based synthetic antiferromagnetic coupling enabled by a W capping or buffer layer, *Sci. Rep.* 6, 21324 (2016).
- [34] Ruderman, M.A. and C. Kittel, Indirect Exchange Coupling of Nuclear Magnetic Moments by Conduction Electrons, *Phys. Rev.* 96, 99 (1954).
- [35] Kasuya, T., A Theory of Metallic Ferromagnetism and Antiferromagnetism on Zeners Model, *Prog. Theor. Phys.* 16, 45 (1956).
- [36] Yosida, K., Magnetic Properties of Cu-Mn Alloys, *Phys. Rev.* 106, 893 (1957).
- [37] Bruno, P. and C. Chappert, Oscillatory Coupling between Ferromagnetic Layers Separated by a Nonmagnetic Metal Spacer, *Phys. Rev. Lett.* 67, 1602 (1991).
- [38] Bruno, P. and C. Chappert, Ruderman-Kittel Theory of Oscillatory Interlayer Exchange Coupling, *Phys. Rev. B* 46, 261 (1992).
- [39] Moritz, J., F. Garcia, J.C. Toussaint, B. Dieny, and J.P. Nozieres, Orange peel coupling in multilayers with perpendicular magnetic anisotropy: Application to (Co/Pt)-based exchange-biased spin-valves, *Europhys. Lett.* 65, 123 (2004).
- [40] Layadi, A. and J.O. Artman, Ferromagnetic resonance in a coupled two-layer system, *J. Magn. Mater.* 92, 143 (1990).